



Hydrothermal crystal growth of 2-D and 3-D barium rare earth germanates: BaREGeO₄(OH) and BaRE₁₀(GeO₄)₄O₈ (RE = Ho, Er)

Kyle Fulle^a, Liurukara D. Sanjeeva^a, Colin D. McMillen^a, Channa R. De Silva^b, Katarina Ruehl^b, Yimei Wen^a, George Chumanov^a, Joseph W. Kolis^{a,*}

^a Department of Chemistry and Center for Optical Materials Science and Engineering Technologies (COMSET), Clemson University, Clemson, SC 29634-0973, USA

^b Department of Chemistry & Physics, Western Carolina University, Cullowhee, NC, 28723, USA

ARTICLE INFO

Article history:

Received 14 February 2018

Received in revised form

8 January 2019

Accepted 14 January 2019

Available online 17 January 2019

Keywords:

Crystal growth

Rare earth compounds

Germanates

X-ray diffraction

ABSTRACT

Two new structural types of BaREGeO₄(OH) and BaRE₁₀(GeO₄)₄O₈ (RE = Ho³⁺, Er³⁺) single crystals were synthesized via high-temperature and high-pressure hydrothermal synthesis. The BaREGeO₄(OH) compounds were found to crystallize in the orthorhombic space group *Pbca*. BaHoGeO₄(OH) is used as a representative of the family with cell parameters of *a* = 5.7175(2) Å, *b* = 10.1556(5) Å, *c* = 10.6189(9) Å and *V* = 964.97(8) Å³. The BaREGeO₄(OH) structure contains a one-dimensional chain of rare-earth polyhedra linked through edge sharing of oxygen atoms. High density BaRE₁₀(GeO₄)₄O₈ crystals crystallize in the monoclinic space group *C2/m* and feature a sheet like arrangement of rare-earth oxide polyhedra with Keggin-like features. BaHo₁₀(GeO₄)₄O₈ is used as a representative of this structure type with cell parameters of *a* = 12.4533(8) Å, *b* = 7.2008(5) Å, *c* = 12.0034(8) Å, *β* = 100.183(2)° and *V* = 1059.43(12) Å³. Barium polyhedra and isolated GeO₄ units aid in connecting the rare earth oxide framework to extend it in three-dimensional (3-D) space. Characterization by single crystal X-ray diffraction and Raman and photoluminescence spectroscopies is reported.

© 2019 Published by Elsevier B.V.

1. Introduction

The pursuit of new inorganic materials with the capacity to host trivalent rare-earth ions for applications such as phosphors and scintillators is an ongoing area of research [1]. In this context, reliable structure determinations are critical to understanding the site symmetry of host materials and anticipating the luminescence spectroscopy of trivalent rare-earth ions in novel compounds. The rare earth silicates have a very rich chemistry and the discovery of new phases shows little indication of slowing down [2–9]. Despite the emergence of the germanate crystals Bi₄Ge₃O₁₂ (BGO) and BiY_{1-x}RE_xGeO₅ (RE = Eu³⁺) as potential scintillators and emitters some years ago, investigation of rare-earth (RE = La–Lu, Y) germanates has not received as much attention as rare-earth silicates [10,11]. It should be noted however, that a number of interesting new alkali rare-earth germanates, including but not limited to, NaEu₃(GeO₄)₂(OH)₂, NaREGeO₄ (RE = Sm–Lu), KLa₉(GeO₄)₆O₂,

Na₅RE₄F(GeO₄)₄ (RE = Pr, Nd), Na₅Nd₄Ge₄O₁₆(OH), Na₂NdGeO₄(OH), K₂TbGe₂O₇, and KEuGe₂O₆ have been prepared recently by solid-state and hydrothermal techniques [12–20]. In general, the differences in structural chemistry between the silicates and germanates can be significant, certainly different enough to justify a detailed comparative study of their respective chemistries [21].

Of the reported alkaline rare-earth germanates, Ca₂Gd₂Ge₂O₉, Ca₃RE₂Ge₃O₁₂ (RE = Pr³⁺–Gd³⁺, Dy³⁺), CaEu₂Ge₃O₁₀, CaRE₂Ge₄O₁₂ (RE = Eu³⁺–Lu³⁺), MgLa₂GeO₆, Be₂RE₂GeO₇ (RE = La³⁺–Er³⁺) and well-studied rare-earth oxy-apatites, no synthetic details of barium rare-earth germanate oxides or oxy-hydroxides have been reported to date, to our knowledge [15,22–29]. The optical properties of the rare earth germanates are of particular interest. For example, the 1.54 μm luminescence of Er³⁺ (4f¹¹) from spin-orbit levels ⁴I_{13/2} → ⁴I_{15/2} is well sought for eye-safe emission [30]. Additionally, upconversion of Ho³⁺ (4f¹⁰) in transparent glass ceramics have been linked to transitions from spin-orbit levels ⁵F₅ → ⁵I₈ which are viable sources for a red emission (650 nm) for use in solid-state displays [31]. These optically active ions have been co-doped into bismuth germanate glasses to allow energy transfer from Er³⁺ ⁴I_{13/2} state to Ho³⁺ ⁵I₇ state for subsequent emission of 2 μm lasing in the

* Corresponding author.

E-mail address: kjoseph@clemson.edu (J.W. Kolis).

eye-safe region [32]. Typically these samples are prepared by conventional solid-state techniques in the form of powders. For detailed studies and optimized performance it is often desirable to prepare the materials as high quality single crystals. As such it is useful to undertake a systematic effort to develop a reliable route to single crystals of rare earth germanates. For the most part metal germanate single crystals have been synthesized using either a flux growth or a hydrothermal method similar to the growth of rare earth silicates. The hydrothermal technique is a particularly attractive method for the examination of germanates because amphoteric oxides tend to grow well in the presence of basic mineralizers [33]. We found that moderately high growth temperatures (600–700 °C) present an excellent intermediate thermal regime, which is cool enough to stabilize a wide range of phases but high enough to induce sufficient solubility for high quality crystal growth.

In this paper we describe the use of a high temperature hydrothermal growth method to prepare single crystals of the first in a series of several new rare earth germanates. We investigate holmium and erbium as the initial rare earth ions because of their interesting optical activity. The introduction of barium ions in the reaction was also included to ascertain the role of counterions in new phases. The presence of an innocent divalent ion performs several functions. It provides a divalent prototype ion that may be systematically replaced with other divalent ions of different size in order to expand the structural possibilities of this class of new phases. The ions can also be subsequently replaced with a more active metals with different magnetic and optical properties. Herein, we report the hydrothermal crystal growth, crystal structure and supporting characterization of two new rare earth germanate phases, BaREGeO₄(OH) and BaRE₁₀(GeO₄)₄O₈ (RE = Ho³⁺–Er³⁺), both of which display interesting new layered structure types.

2. Experimental

2.1. Hydrothermal crystal growth

The title compounds BaREGeO₄(OH) and BaRE₁₀(GeO₄)₄O₈ (RE = Ho³⁺–Er³⁺) were prepared through the direct reaction of BaO, RE₂O₃ and GeO₂ powders via high temperature and high pressure hydrothermal synthesis. As a typical example, BaHoGeO₄(OH) and BaHo₁₀(GeO₄)₄O₈ were prepared by combining BaO (36 mg, 233 mmol; Alfa Aesar, 99.0%), Ho₂O₃ (74 mg, 195 mmol; HEFA Rare Earth, 99.99%) and GeO₂ (41 mg, 389 mmol; Alfa Aesar, 99.9%) in a 3:2.5:5 molar ratio, respectively. The starting materials were reacted isothermally at 650 °C for 7 days in welded silver (99.9%) (1/4" x 2.5") ampoules loaded into a Tuttle cold seal autoclave constructed from Inconel 718 material. The ampoules were loaded with the appropriate component oxide feedstock and weld sealed from both ends after addition of 0.4 mL of 6 M CsOH as a mineralizer. Upon completion of reaction, the silver ampoules were opened and washed with DI water. In each reaction, BaRE₁₀(GeO₄)₄O₈ and BaREGeO₄(OH) crystals (Fig. 1) constituted an approximate 75/25 ratio of products, respectively. The major product, BaRE₁₀(GeO₄)₄O₈, formed as plate-like crystals up to 2.5 mm in size. Crystals of the minor product, BaREGeO₄(OH), were produced as block-like polyhedra, up to 0.75 mm in size. The crystals could be distinguished by visual inspection and manually separated for characterization. The observed morphologies are consistent with those calculated based on the single crystal structures (Supplementary Information, Fig. S1).

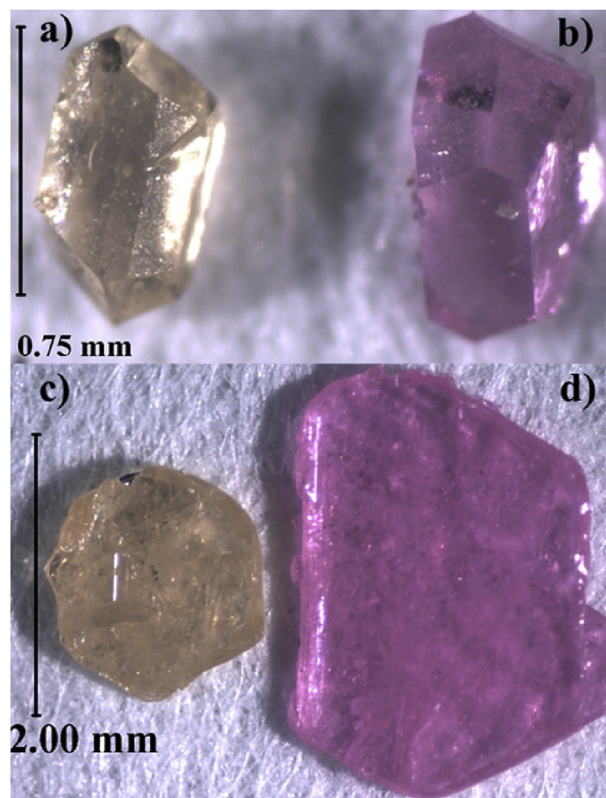


Fig. 1. Crystal growth of new barium rare-earth germanates: a) BaHoGeO₄(OH), b) BaErGeO₄(OH), c) BaHo₁₀(GeO₄)₄O₈ and d) BaEr₁₀(GeO₄)₄O₈ single crystals.

2.2. Structural characterization

Single crystal structure characterization was conducted using a Bruker D8 Venture single crystal diffractometer with an Incoatec Mo K α microfocus source and Photon 100 CMOS detector. Data were collected at room temperature using ϕ and ω scans, and subsequently processed and scaled using the Apex3 (SAINT and SADABS) software suite [34]. Space group determinations were unambiguously made based on the systematic absences. The structures were solved by direct methods and refined to convergence by full-matrix least squares on F^2 using the SHELXTL software suite [35]. All atoms were refined anisotropically. The structure of BaRE₁₀(GeO₄)₄O₈ (RE = Ho, Er) was solved as a two-component non-merohedral twin using the program cell_now to distinguish the twin contributions and TWINABS to integrate the component reflections [36]. For BaRE₁₀(GeO₄)₄O₈ the major and minor twin component contributed 85.5/14.5% for Ho³⁺, and 50.5/49.5% for Er³⁺. Structural data for the title compounds are shown in Table 1. Selected bond lengths and the corresponding bond valence sum calculations are given in the Supplementary Information (SI), Tables S1–S2.

Energy dispersive X-ray analysis (EDX) was used to confirm the presence of Ba²⁺ (instead of Cs⁺ having similar size and electron density) in both structure types and to support the assigned ratio of metals (SI, Figs. S2–S5). EDX was collected on an Oxford INCA EDX analyzer connected to a Hitachi SU6600 scanning electron microscope with a Cu standard. The observed non-hydrogen elemental compositions in atomic percent are as follows, with calculated compositions reported parenthetically: BaHo₁₀(GeO₄)₄O₈: O 64.4 (61.5), Ho 23.8 (25.6), Ge 9.1 (10.3), Ba 2.7 (2.6); BaEr₁₀(GeO₄)₄O₈: O 60.1 (61.5), Er 26.6 (25.6), Ge 10.4 (10.3), Ba 2.9 (2.6); BaHoGeO₄OH: O 53.6 (62.5), Ho 15.7 (12.5), Ge 14.8 (12.5), Ba 15.9 (12.5);

Table 1

Crystallographic data of rare earth germanates and germanate hydroxides determined by single crystal X-ray diffraction.

empirical formula	BaHo ₁₀ (GeO ₄) ₄ O ₈	BaEr ₁₀ (GeO ₄) ₄ O ₈	BaHoGeO ₄ (OH)	BaErGeO ₄ (OH)
formula weight (g/mol)	2461.00	2484.30	455.87	458.20
crystal system	monoclinic	monoclinic	orthorhombic	orthorhombic
space group, <i>Z</i>	<i>C2/m</i> (no.12), 2	<i>C2/m</i> (no.12), 2	<i>Pbca</i> (no.61), 8	<i>Pbca</i> (no.61), 8
temperature, K	298(2)	298(2)	298(2)	298(2)
crystal size (mm)	0.08 × 0.10 × 0.10	0.07 × 0.07 × 0.07	0.02 × 0.05 × 0.07	0.08 × 0.08 × 0.09
<i>a</i> , Å	12.4972(5)	12.4533(8)	5.7175(2)	5.7100(2)
<i>b</i> , Å	7.2444(3)	7.2008(5)	10.1556(5)	10.1511(5)
<i>c</i> , Å	12.0170(5)	12.0034(8)	16.6189(9)	16.5766(8)
β , °	100.249(2)	100.183(2)	—	—
volume, Å ³	1070.60(8)	1059.43(12)	964.97(8)	960.83(7)
calculated density (μg/m ³)	7.634	7.788	6.276	6.335
Θ range for data	3.26–30.58	3.28–28.29	4.01–26.50	4.02–26.49
data/restraints/parameters	2443/6/107	1790/12/107	1002/1/77	993/1/77
final <i>R</i> [<i>I</i> > 2σ(<i>I</i>)] <i>R</i> ₁ , <i>wR</i> ₂	0.0362, 0.0785	0.0440, 0.1184	0.0213, 0.0382	0.0161, 0.0316
final <i>R</i> (all data) <i>R</i> ₁ , <i>wR</i> ₂	0.0425, 0.0810	0.0483, 0.1216	0.0296, 0.0404	0.0195, 0.0325
goodness-of-fit on <i>F</i> ²	1.131	1.087	1.102	1.196

BaErGeO₄OH: O 59.7 (62.5), Er 12.2 (12.5), Ge 15.0 (12.5), Ba 13.0 (12.5). Powder X-ray diffraction (PXRD) was performed using a Rigaku Ultima IV diffractometer with CuK α radiation ($\lambda = 1.5406$ Å) at 0.02° intervals at a rate of 0.25°/min from 5 to 65°. Powder patterns of the reaction products from the representative erbium reaction, including comparisons to the calculated patterns generated from the single crystal structures are given in Fig. 2. The PXRD analysis of hand-selected crystals of BaEr₁₀(GeO₄)₄O₈ is shown in the SI, Fig. S6.

2.3. Raman single crystal scattering

Raman scattering was used to confirm the presence or absence of hydroxide groups in the structures (SI, Fig. S7), as well as evaluate the vibrational modes resulting from the GeO₄ units. Raman measurements were performed using an Olympus IX71 inverted microscope with a 20× objective lens coupled to a TRIAX 552 spectrometer equipped with a thermoelectrically cooled CCD detector (Andor Technology, Model DU420A-BV) operating at −60 °C. An argon ion laser (Innova 100, Coherent) was used to excite the Raman signal with 514.5 nm light in a 180° backscattering geometry. A PR-550 broadband polarization rotator (Newport Corp.) was

used to rotate the polarization of the incident laser source. All spectra were processed and figures prepared with Spectra-Solve for Windows software (Las Tek Pty. Ltd.) Data were collected with a laser output power of 100–200 mW with a 2-minute integration time.

2.4. Photoluminescence studies

Photoluminescence studies were carried out using a Horiba Jobin Yvon LabRAM-HR Evolution Raman spectrometer equipped with an 800 mm monochromator, a Rayleigh-rejection filter, an Olympus BX41 optical microscope, and a TE-cooled charge-coupled device (CCD) detector. Crystals of BaRE₁₀(GeO₄)₄O₈ (RE = Ho³⁺–Er³⁺) were mounted on a glass slide for measuring steady state luminescence at room temperature. Excitation of the samples were done using the 457.9 nm excitation from a Spectra Physics 2065-7S Argon laser with a power of 100 mW and the emission was collected in the wavelength range of 400–900 nm. A 50× long working-distance objective was used to focus the laser light on to the sample surface. The lateral resolution was on the order of 5 μm. The depth resolution was on the order of 10–20 μm.

3. Results and discussion

3.1. Crystal structure of BaREGeO₄(OH) (RE = Ho³⁺–Er³⁺)

The BaREGeO₄(OH) (RE = Ho³⁺–Er³⁺) compounds in the current study crystallize in the orthorhombic space group *Pbca* (No. 61). The two compounds are isostructural with one another, with the Er³⁺ analog exhibiting slightly contracted cell parameters compared to Ho³⁺, Table 1. BaHoGeO₄(OH) is used as a representative of the family with cell parameters of *a* = 5.7175(2) Å, *b* = 10.1556(5) Å, *c* = 10.6189(9) Å and *V* = 964.97(8) Å³. The structure is based on building block units of HoO₇, BaO₁₀ and isolated GeO₄ tetrahedra, Fig. 3. All atoms reside on general crystallographic positions with 8c Wyckoff symmetry. As seen in Figs. 3a and 4a, infinite zigzag chains of HoO₇ polyhedra run parallel to the *a*-axis via edge sharing of O(4) and O(5) atoms and are the key structural component to the framework. Each GeO₄ unit coordinates four HoO₇ polyhedra via corner-sharing of O(1) and O(3), and edge-sharing of O(2) and O(4) oxygen atoms, and each HoO₇ polyhedron likewise coordinates four GeO₄ units (Fig. 4b) to form rare earth germanate slabs in the *ab* plane (Fig. 2).

Barium atoms reside between the slabs of corner- and edge-shared HoO₇ and GeO₄ polyhedra, creating an overall three-dimensional network. These atoms exist as irregular polyhedra

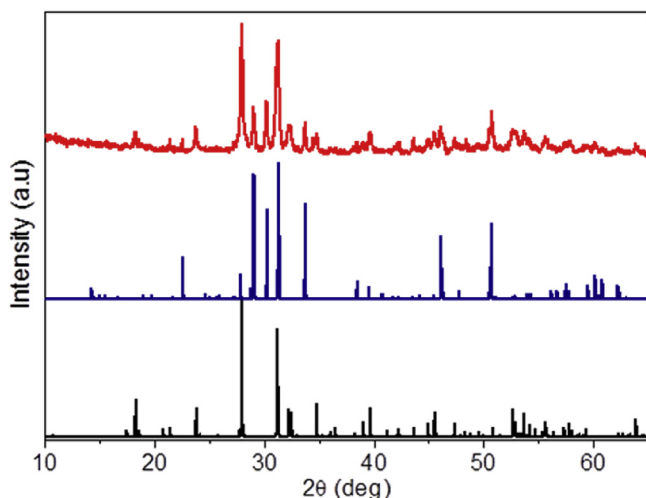


Fig. 2. Composite reaction product (top, red) of the hydrothermal reaction of $3\text{BaO} + 2.5\text{Er}_2\text{O}_3 + 5\text{GeO}_2$, indicating a mixture of BaEr₁₀(GeO₄)₄O₈ (calculated, middle, blue) and BaErGeO₄(OH) (calculated, bottom, black). (For interpretation of the references to colour in this figure legend, the reader is referred to the Web version of this article.)

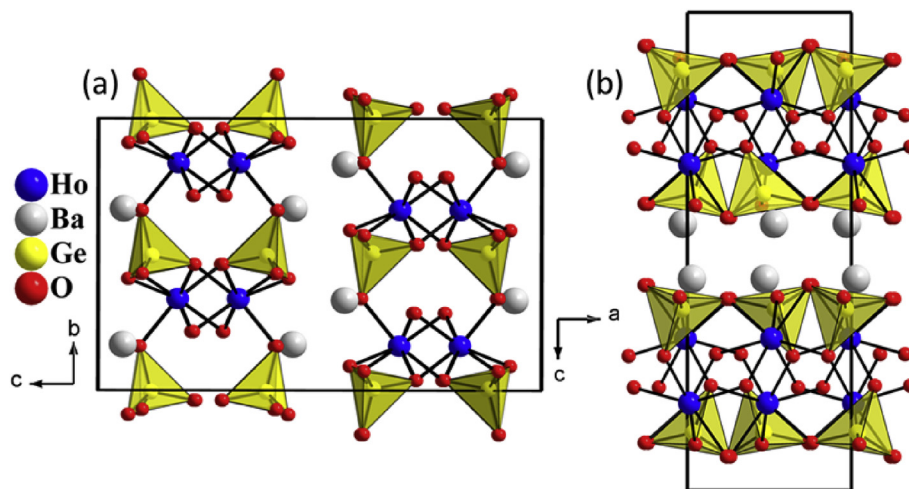


Fig. 3. a) Isolated GeO_4 units connect holmium oxide polyhedra in the (001) plane with barium atoms residing between layers. b) Holmium oxide polyhedra extending along the [100] direction through edge sharing of oxygen atoms to form a one-dimensional rare-earth oxide chain.

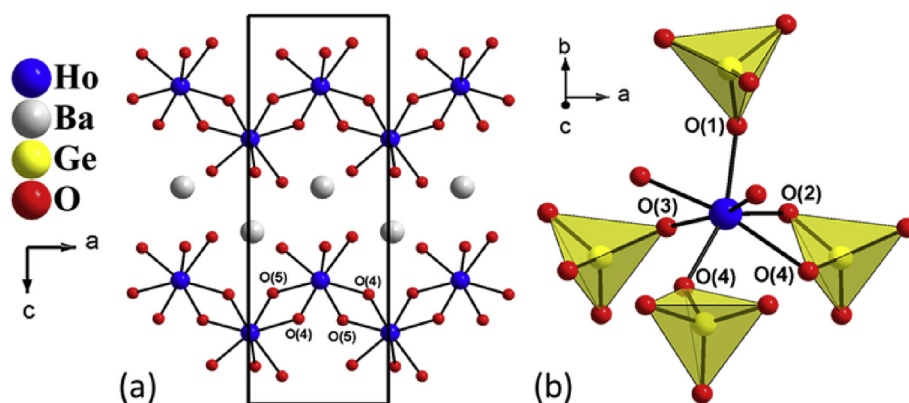


Fig. 4. a) Ho(1)O_7 polyhedra forming infinite chains separated by interstitial barium atoms and connected via edge-sharing of O(4) and O(5) oxygen atoms in the (010) plane. b) Each Ho(1)O_7 polyhedra coordinates four GeO_4 units through corner-sharing of O(1), O(3), O(4) and edge-sharing of O(2)/O(4) oxygen atoms, shown just off [001] direction.

coordinated by oxygen, with Ba—O distances between 2.579(4)—3.241(4) Å and averaging 2.94 Å. The HoO_7 polyhedra form a distorted trigonal prismatic, square-face mono-capped geometry with Ho—O bond lengths ranging from 2.262(4)—2.433(4) Å with an average of 2.33 Å. The GeO_4 tetrahedra exhibit bond lengths ranging from 1.742(4)—1.771(4) Å with an average distance of 1.75 Å. Bond valence sum calculations resulted in values of 1.94, 3.10, and 3.93 for Ba^{2+} , Ho^{3+} , and Ge^{4+} , respectively, consistent with the assigned oxidation states [37,38]. Assignment of one hydroxide group is necessary to complete the charge balance of the compound. The O(5) oxygen atom was found to be the hydroxide unit based on bond valence sum considerations. The O(5) oxygen atom does not support a bond to the germanium atom, and serves as a bridging oxygen atom within the chains of HoO_7 units. In the case of O(5), its bond valence sum is 1.15, compared to the other oxygen atoms that exhibit values of 1.79–2.11, supporting the assignment of OH^- and O^{2-} , respectively (SI, Table S2). The arrangement of the hydroxide group is favorable for hydrogen bonding between neighboring chains of HoO_7 units via O(5)—H(5)—O(4) interactions, providing additional reinforcement of the slabs. The presence of hydroxide group is supported by the infrared analysis of $\text{BaHoGeO}_4(\text{OH})$ and $\text{BaErGeO}_4(\text{OH})$ as well as the single crystal Raman scattering indicating a strong stretching mode at 3420 cm^{-1} for $\text{BaHoGeO}_4(\text{OH})$, (SI, Fig. S7).

The formula of these new barium rare-earth oxy-hydroxides discussed herein are somewhat reminiscent of the sodium rare-earth germanate species $\text{Na}_2\text{NdGeO}_4(\text{OH})$, synthesized by mild hydro-flux of sodium hydroxide [17]. Both structures exhibit one-dimensional zigzag chains of rare-earth polyhedra. However, these structures are not isostructural as $\text{Na}_2\text{NdGeO}_4(\text{OH})$ chains interconnect via corner sharing of O(4) atoms forming an intricate rare-earth framework, while $\text{BaREGeO}_4(\text{OH})$ exhibits truly isolated one-dimensional chains interconnected through isolated GeO_4 building blocks.

3.2. Crystal structure of $\text{BaRE}_{10}(\text{GeO}_4)_4\text{O}_8$ ($\text{RE} = \text{Ho}^{3+}\text{--Er}^{3+}$)

The $\text{BaRE}_{10}(\text{GeO}_4)_4\text{O}_8$ ($\text{RE} = \text{Ho}^{3+}\text{--Er}^{3+}$) crystals represent, to our knowledge, the first barium rare earth germanate oxide to be structurally characterized. The structure is built from BaO_8 , HoO_6 , HoO_7 and GeO_4 building blocks. The Ho^{3+} and Er^{3+} analogs are again isostructural with one another, where the unit cell parameters for the Er^{3+} species are slightly contracted. $\text{BaHo}_{10}(\text{GeO}_4)_4\text{O}_8$ is used as a representative of this structure type with cell parameters of $a = 12.4533(8)$ Å, $b = 7.2008(5)$ Å, $c = 12.0034(8)$ Å, $\beta = 100.183(2)^\circ$ and $V = 1059.43(12)$ Å³. The use of concentrated CsOH as a mineralizer for the synthesis required a systematic approach to accurately assign the structure as $\text{BaRE}_{10}(\text{GeO}_4)_4\text{O}_8$.

over $\text{CsRE}_{10}(\text{GeO}_4)_4\text{O}_7(\text{OH})$. Energy dispersive X-ray spectroscopy and single crystal Raman spectroscopy were employed to deduce the final structural assignment. The absence of cesium from EDX of single crystals of $\text{BaHo}_{10}(\text{GeO}_4)_4\text{O}_8$ and $\text{BaEr}_{10}(\text{GeO}_4)_4\text{O}_8$, in addition to an absence of hydroxide stretching modes in the Raman spectroscopy, leaves no ambiguity to the reported barium rare-earth oxides (SI, Figs. S1–S2, S7).

The structure type contains four unique crystallographic Ho^{3+} sites: $\text{Ho}(1)\text{O}_7$ (4i), $\text{Ho}(2)\text{O}_7$ (4i), $\text{Ho}(3)\text{O}_7$ (8j), and $\text{Ho}(4)\text{O}_6$ (4g) with $\text{Ho}(1)/\text{Ho}(2)$ residing on mirror planes and $\text{Ho}(4)$ residing on a 2-fold symmetry site. The Ho–O bond distances range from 2.187(5) to 2.490(7) Å for the four holmium oxide polyhedra. The compound forms a complex network of HoO_6 and HoO_7 polyhedra that form sheets propagating along the *ab*-plane, Fig. 5.

Within the rare-earth oxide framework, two distinct modes of connectivity are observed. The first framework is built up of $\text{Ho}(4)$ polyhedra that interconnect through edge-sharing of alternating O(4) and O(9) atoms in the *ab*-plane, Fig. 6a. These chains interconnect through $\text{Ho}(2)$ polyhedra coordinating through μ_3 bridging of O(2), O(4) and O(9) to construct a honeycomb-type lattice, also shown in Fig. 6a. Simultaneously, $\text{Ho}(1)$ and $\text{Ho}(3)$ polyhedra form a planar network constructed from edge sharing of O(1), O(3), O(7) and O(8) with μ_3 bridging of O(5) and O(6), Fig. 6b. This contains distorted channels along the *c*-axis in which barium atoms coordinate. The $\text{Ho}(1)$ and $\text{Ho}(3)$ polyhedra form a cap with the $\text{Ho}(2)/\text{Ho}(4)$ honeycomb lattice residing within this cap and interconnecting through overall μ_4 bridging of O(2) and O(4). This framework of holmium oxide polyhedra forms a sheet which propagates in the *ab*-plane with barium atoms separating the layers and providing the necessary charge balance.

Isolated GeO_4 tetrahedra support the solid-state framework by connecting the holmium oxide sheets along the *c*-axis (Figs. 5b and 7). Two crystallographically distinct germanium sites, $\text{Ge}(1)\text{O}_4$ and $\text{Ge}(2)\text{O}_4$, reside on 4i Wyckoff sites with mirror symmetry. The Ge–O bond distances range from 1.734(9) to 1.748(9) Å for the two germanium sites. $\text{Ge}(1)\text{O}_4$ coordinates nine holmium polyhedra and resides in the same plane as the rare earth oxide sheets, Fig. 7a. $\text{Ge}(1)\text{O}_4$ coordinates a trimeric unit of $\text{Ho}(2)$ and two $\text{Ho}(4)$ atoms through bridging of O(9) above the tetrahedral site in the *ab*-plane. Additionally, $\text{Ge}(1)\text{O}_4$ coordinates six holmium centers, (four $\text{Ho}(3)$ and two $\text{Ho}(1)$ atoms), through corner-shared O(1) and O(3) oxygen atoms below the *ab*-plane, Fig. 7a. The $\text{Ge}(1)\text{O}_4$ tetrahedra link the two distinct rare-earth frameworks while $\text{Ge}(2)\text{O}_4$ tetrahedra help create distorted channels where barium atoms reside. The $\text{Ge}(2)\text{O}_4$ tetrahedra coordinate two trimeric units, (two $\text{Ho}(3)$ and one $\text{Ho}(1)$)

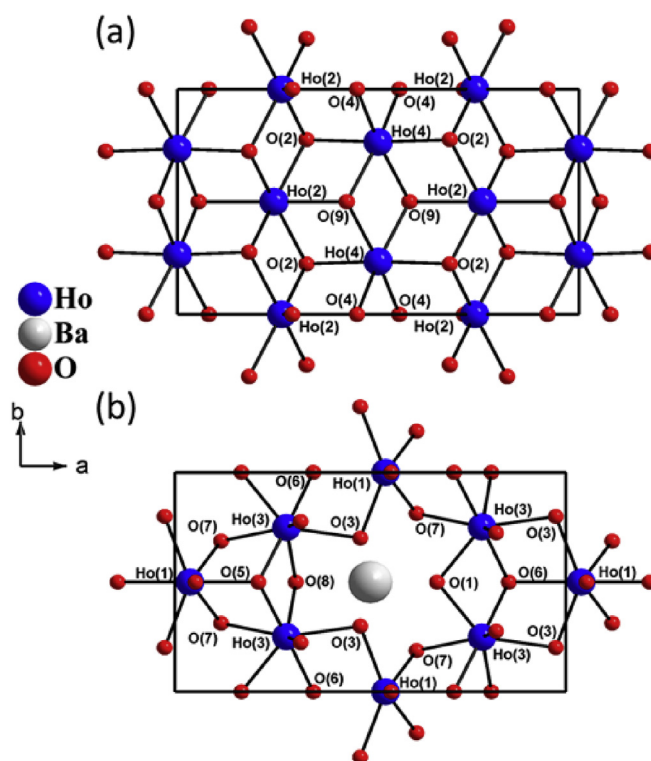


Fig. 6. (a) $\text{Ho}(2)$ and $\text{Ho}(4)$ polyhedra forming a honeycomb-type of arrangement visible along the [001] direction. (b) $\text{Ho}(1)$ and $\text{Ho}(3)$ polyhedra creating distorted channels with Ba^{2+} ions coordinating the center to provide additional structural support and charge balance.

atoms), in the *ab*-plane through bridging of O(6) above the tetrahedral site and below through edge-sharing of O(7) and O(8) atoms, Fig. 7b. $\text{Ge}(2)\text{O}_4$ tetrahedra reside between the rare-earth layers with neighboring barium atoms, thus strengthening the layered structure. The $\text{Ge}(2)\text{O}_4$ tetrahedron alternates in up/down direction relative to the *c*-axis while propagating throughout the *ab*-plane, Fig. 5b. Bond valence sum calculations resulted in values of 1.72, 3.06, 2.99, 2.94, 2.95, 4.08, 4.03 for $\text{Ba}(1)$, $\text{Ho}(1)$, $\text{Ho}(2)$, $\text{Ho}(3)$, $\text{Ho}(4)$, $\text{Ge}(1)$ and $\text{Ge}(2)$, respectively, which are consistent with the assigned oxidation states and charge-balanced composition.

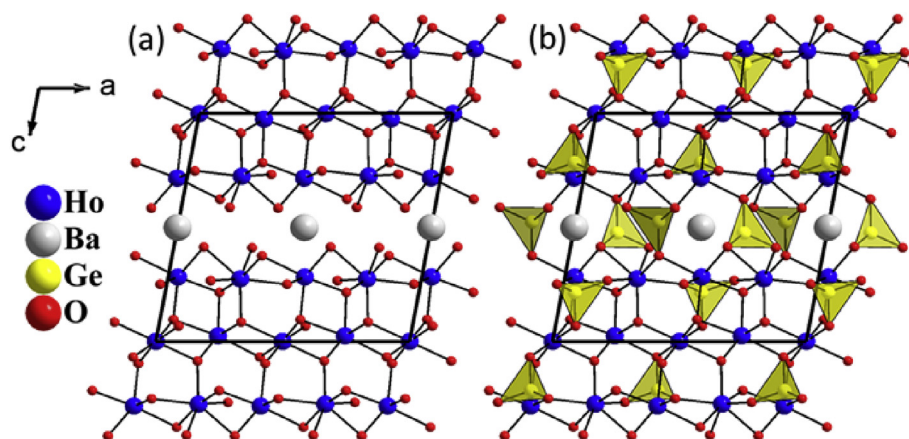


Fig. 5. $\text{BaHo}_{10}(\text{GeO}_4)_4\text{O}_8$ view along the [010] projection. (a) Sheet-like arrangement of holmium oxide polyhedra extending in the *ab*-plane with Ba^{2+} ions occupying void between layers. (b) Isolated GeO_4 units stabilize the rare-earth framework and encapsulate the Ba^{2+} ions in channels along [010] direction.

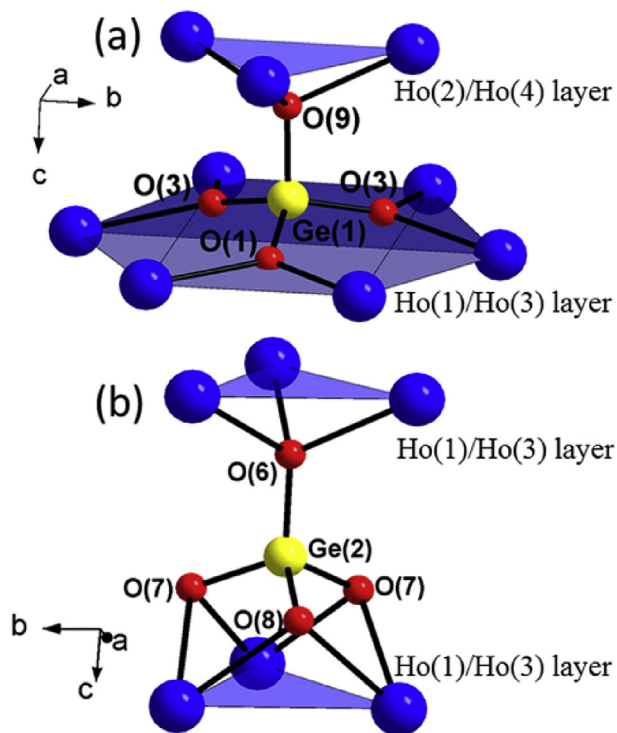


Fig. 7. (a) Ge(1)O₄ coordination highlighting bridging between Ho(2)/Ho(4) and Ho(1)/Ho(3) layers. (b) Ge(2)O₄ coordination between Ho(1)/Ho(3) layers just off [100] direction. Full holmium coordination polyhedra are omitted for clarity.

3.3. Single crystal Raman characterization

BaHoGeO₄(OH) and BaHo₁₀(GeO₄)₄O₈ are examined as representatives of each new structure type by single crystal Raman scattering. Factor group analysis for BaHoGeO₄(OH) orthorhombic structure (*Pbca*, *Z* = 8), factor group D_{2h}^{15} , reveals that the normal modes are distributed among the following irreducible representations for the elementary unit cell: $27A_g + 27A_u + 27B_{1g} + 27B_{1u} + 27B_{2g} + 27B_{2u} + 27B_{3g} + 27B_{3u}$. Here, B_{1u} , B_{2u} and B_{3u} can be assigned to acoustic modes, $26B_{1u} + 26B_{2u} + 26B_{3u}$ to IR active modes, and $27A_g + 27B_{1g} + 27B_{2g} + 27B_{3g}$ to Raman active modes. Since the Ge—O bonds are much stronger than the Ho—O bonds, and exhibit distortion away from ideal *T_d* symmetry, simplification of the Raman active modes to focus on the GeO₄ tetrahedra is appropriate.

For each free GeO₄ group, nine internal Raman vibrational modes are expected from the general formula $3n-6$. The GeO₄ groups in BaHoGeO₄(OH) adopt *C₁* point group symmetry, and internal vibrations can be described by *A* Raman active modes. BaHoGeO₄(OH) exhibits a strong Raman signal at 785 cm^{−1} which has been assigned to the symmetric ν_1 stretching modes and asymmetric ν_3 stretching modes observed for bands from 700 to 800 cm^{−1}, Fig. 8a. Bands in the 400–500 cm^{−1} region have been assigned to the ν_4 bending internal modes of the GeO₄ building block.

Factor group analysis of monoclinic BaHo₁₀(GeO₄)₄O₈ (*C₂/m*, *Z* = 2), factor group C_{2h}^3 , reveals the normal modes are distributed among the following irreducible representations for the elementary unit cell: $33A_g + 24A_u + 24B_g + 36B_u$. From these modes, two modes should be classified as acoustic ($A_u + 2B_u$). The IR active modes are $23A_u + 34B_u$, while $33A_g + 24B_g$ represent Raman active modes. Fig. 8b reveals three distinct peaks from 700 to 810 cm^{−1}, with an intense Raman peak at 765 cm^{−1}. Again, these peaks have

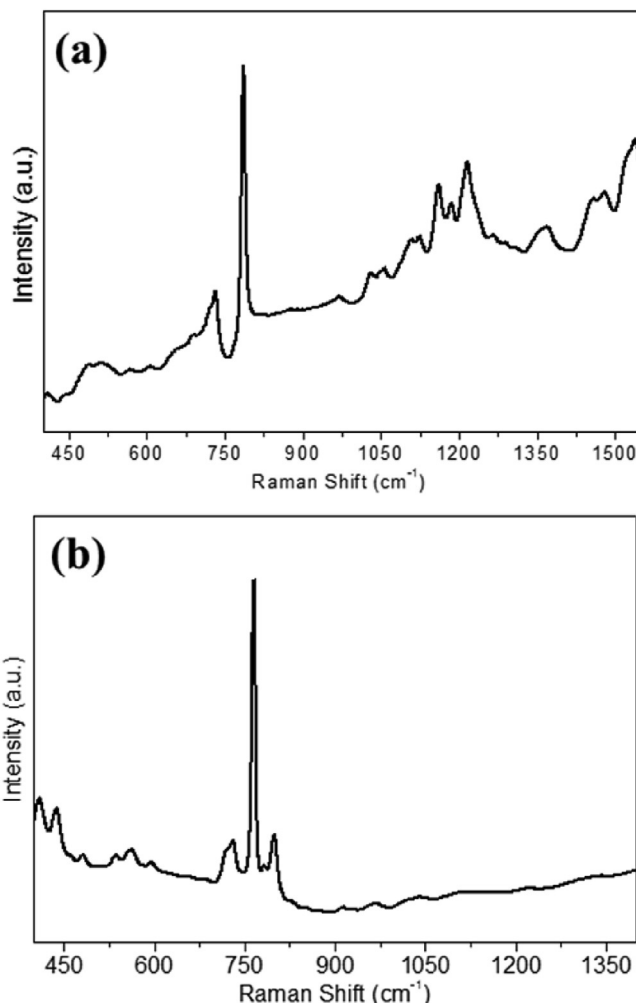


Fig. 8. Single crystal Raman scattering of (a) BaHoGeO₄(OH) and (b) BaHo₁₀(GeO₄)₄O₈.

been assigned to symmetric ν_1 stretching modes and asymmetric ν_3 stretching modes. Bands in the 400–500 cm^{−1} region are assigned to the ν_4 bending internal modes of the germanate. This is commensurate with known rare-earth apatite La_{8+x}Ba_{2-x}(GeO₄)₆O_{2+x/2} (*x* = 0 and 1.2) structural types, which also display isolated [GeO₄]^{4−} building blocks, and scattering bands were assigned these corresponding modes [39,40].

3.4. Photoluminescence studies of BaHo₁₀(GeO₄)₄O₈ and BaEr₁₀(GeO₄)₄O₈

Photoluminescence spectra of BaRE₁₀(GeO₄)₄O₈ (RE = Ho³⁺, Er³⁺) crystals were collected using 457.9 nm laser excitation are shown in Fig. 9. A laser excitation of 457.9 nm was chosen for direct excitation of Er³⁺ and Ho³⁺ ions via *f* to *f* electronic transitions. The excitation wavelength overlaps with the $^4I_{15/2}$ to $^4F_{5/2}$ electronic transition and the 5F_3 to 5I_8 electronic transition of Er³⁺ and Ho³⁺ ions, respectively. The excited energy can then be transferred to lower excited levels of each metal ion exhibiting the observed luminescence of the crystals.

The emission spectrum in Fig. 9a indicates an intense peak in the green spectral range (between 550 and 570 nm) which is characteristic of Er³⁺ ions present in the BaEr₁₀(GeO₄)₄O₈ crystal. This peak can be associated with the $^4S_{3/2}$ to $^4I_{15/2}$ transition of Er³⁺ ions. The peaks centered at around 540 nm and 675 nm can be

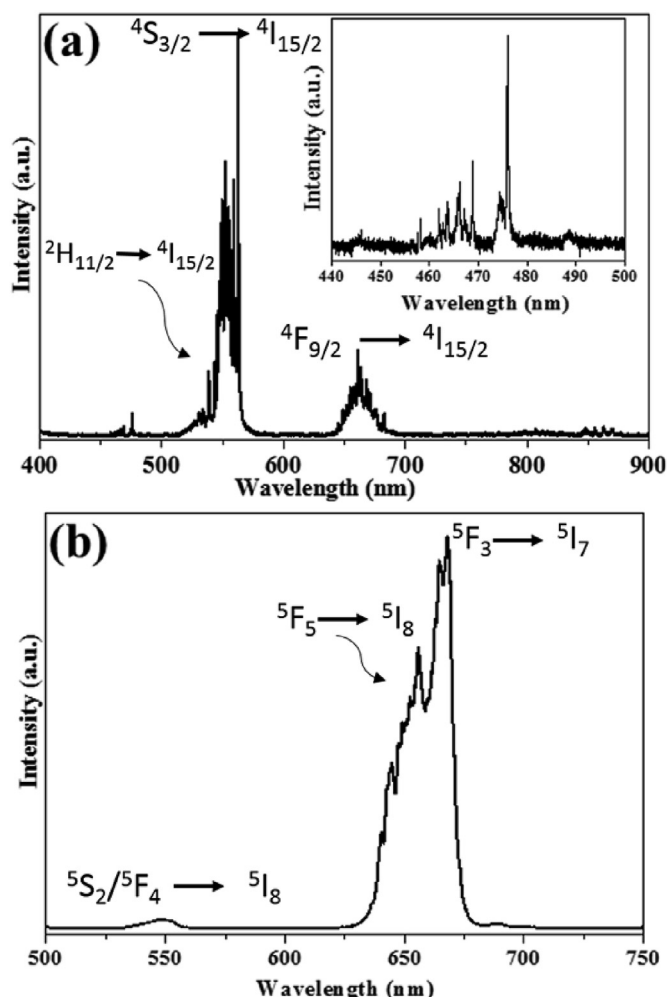


Fig. 9. Solid-phase photoluminescence emission spectra of (a) $\text{BaEr}_{10}(\text{GeO}_4)_4\text{O}_8$ and (b) $\text{BaHo}_{10}(\text{GeO}_4)_4\text{O}_8$ crystals using 457.9 nm laser excitation (inset of (a) shows a detailed view of the region from 440 to 500 nm).

associated with $^2\text{H}_{11/2} \rightarrow ^4\text{I}_{15/2}$ and $^4\text{F}_{9/2} \rightarrow ^4\text{I}_{15/2}$ transitions of Er^{3+} ions, respectively. Similar emission patterns were observed for Er^{3+} ions in silicate frameworks containing barium ions [41]. Fig. 9b shows the characteristic emission peaks of Ho^{3+} ions present in the $\text{BaHo}_{10}(\text{GeO}_4)_4\text{O}_8$ crystal. The dominant peak in the red spectral region (630–675 nm) is associated with $^5\text{F}_3 \rightarrow ^5\text{I}_7$ transition. A similar peak pattern is observed for Ho^{3+} containing silicate crystals containing barium ions [41]. Similar luminescent peak patterns observed for our crystals (containing germanates) and the literature reported crystals (containing silicates) may be due to the diminished nature of the matrix effects. Thus, the electronic structure of the Er^{3+} and Ho^{3+} ions are minimally influenced by the matrix in germanates compared to that in silicates.

3.5. Comparison of germanate and silicate chemistries

While the rare earths have often been viewed as a monotonic chemical block, their structural chemistry in the presence of oxyanion building blocks such as silicates indicates that this is not true [2,42]. In particular the chemistry across the f-block ion silicates in hydrothermal aqueous fluids has consistently shown an unexpectedly diverse behavior, leading to the emergence of a wide range new materials with interesting solid-state frameworks. Recently, we investigated the chemistry of barium rare-earth silicates

($\text{Ba}_2\text{RE}_2\text{Si}_4\text{O}_{13}$) ($\text{RE} = \text{La}^{3+}\text{--}\text{Ho}^{3+}$) and barium rare-earth silicate fluorides ($\text{Ba}_2\text{RE}_2\text{Si}_4\text{O}_{12}\text{F}_2$) ($\text{RE} = \text{Er}^{3+}\text{--}\text{Lu}^{3+}$) in high temperature and high-pressure hydrothermal conditions to determine the effect of rare-earth size on phase transitions between these structures [42]. In a logical extension of this work we began investigation the chemistry of rare earth germanates in hydrothermal fluids, typically using aqueous bases such as CsOH as a mineralizer. The tetrahedral building blocks of silica and germanium oxide also show very different structural chemistry despite belonging to the same periodic group and displaying similar coordination chemistry. The structural chemistry of metal germanates is further complicated by the fact that, unlike silicates, germanates often display coordination environments other than tetrahedral (five- and six-coordinate), which makes the possible phase space even greater [43].

Interestingly, although the polygermanates show a very rich structural chemistry in Ge-O frameworks, there are fewer examples of germanates directly coordinated to rare earth metal centers where the germanate groups are not limited to tetrahedra or polymeric tetrahedra like the silicates. There are a number of interesting uranium compounds with unusual polygermanate building blocks beyond the conventional tetrahedra that were synthesized using high temperature hydrothermal methods [44,45]. These interesting compounds strongly suggest that rare earth germanates with non-tetrahedral building blocks can be synthesized and isolated under appropriate hydrothermal conditions. We began a systematic examination of the phase space of rare earth germanates under these typical high temperature hydrothermal reaction conditions with the belief that a menu of isolated tetrahedral germanates, various polymeric germanate clusters and of non-tetrahedral germanate building blocks, along with a wide variety of coordination environments of the rare earth ions, would combine to provide an almost infinite possibility of new structure types. Our long term goal is to be able to provide some degree of predictability to this chemistry in order to extract the maximum degree of performance of luminescent, lasing, magnetic and other useful properties of the germanates. We feel that a high temperature hydrothermal approach is an attractive one because of the chemical flexibility that it provides as well as its ability to form high quality crystals of materials whose parent oxide building blocks are extremely refractory in nature [46]. As we expected the approach does lead to a wide range on new materials and these are currently under investigation.

4. Summary and conclusions

In this paper we describe our initial results using two rare earth (Er, Ho) ions near the middle of the f-block that typically display interesting spectroscopic properties which leads to two interesting new structural types. The reaction of barium oxide, select rare-earth oxides, and germanium oxide in hydrothermal fluids was done using a hydroxide mineralizer of 6 M CsOH. Two new stable products were isolated. $\text{BaREGeO}_4(\text{OH})$ ($\text{RE} = \text{Ho, Er}$) single crystals formed as a minor hydrothermal product as good single crystals (0.75 mm). This new structure type displays an isolated one-dimensional chain of rare-earth polyhedra that are connected through edge sharing of oxygen atoms of isolated GeO_4 building blocks forming sheets with Ba^{2+} ions between layers. A second product major product $\text{BaRE}_{10}(\text{GeO}_4)_4\text{O}_8$ ($\text{RE} = \text{Ho, Er}$) displays a unique sheet-like arrangement involving four unique rare-earth sites separated by Ba^{2+} ions and coordinated by isolated GeO_4 units. This material grows as quite large single crystals, exceeding 2 mm in size.

Compared to recently investigated rare earth silicates, the phase stability of the barium rare-earth germanates appears much more complex. While the SiO_4 and GeO_4 building blocks display many of

the same coordination features, the hydrothermal chemistry of these rare-earth building blocks are thus far quite different. The IR, Raman and photoluminescence spectroscopy also correlated well with the observed structures. The introduction of barium ions in the chemistry provides an additional chemical and structural variability. To our knowledge this is the first example of a rare earth germanate containing a barium ion (excepting mixed alkali-alkaline earth rare earth germanates). These preliminary results suggest that a wide range of new rare earth germanates can be isolated as large single crystals and their magnetic and optical properties can be studied.

Acknowledgment

The authors thank the Department of Energy Basic Energy Sciences DE-SC0014271 for financial support.

Appendix A. Supplementary data

Supplementary data to this article can be found online at <https://doi.org/10.1016/j.jallcom.2019.01.185>.

References

- [1] M.S. Wickleder, Inorganic lanthanide compounds with complex anions, *Chem. Rev.* 102 (2002) 2011–2088, <https://doi.org/10.1021/cr010308o>.
- [2] M. Wierzbicka-Wieczorek, U. Kolitsch, E. Tillmanns, Synthesis and structural study of five new trisilicates, BaRE₂Si₃O₁₀ (RE = Gd, Er, Yb, Sc) and SrY₂-Si₃O₁₀, including a review on the geometry of the Si₃O₁₀ unit, *Eur. J. Mineral.* 22 (2010) 245–258, <https://doi.org/10.1127/0935-1221/2010/0022-1969>.
- [3] J. Felsche, The crystal chemistry of the rare-earth silicates, in: *Rare Earths*, Springer, Berlin, Heidelberg, 1973, pp. 99–197, https://doi.org/10.1007/3-540-06125-8_3.
- [4] M. Wierzbicka-Wieczorek, U. Kolitsch, E. Tillmanns, Ba₂Gd₂(Si₄O₁₃): a silicate with finite Si₄O₁₃ chains, *Acta Crystallogr. C* 66 (2010) i29–i32, <https://doi.org/10.1107/S0108270110002842>.
- [5] I. Vidican, M.D. Smith, H.-C. zur Loye, Crystal growth, structure determination, and optical properties of new potassium-rare-earth silicates K₃RESi₂O₇ (RE=Gd, Tb, Dy, Ho, Er, Tm, Yb, Lu), *J. Solid State Chem.* 170 (2003) 203–210, [https://doi.org/10.1016/S0022-4596\(02\)00029-4](https://doi.org/10.1016/S0022-4596(02)00029-4).
- [6] S.M. Haile, B.J. Wuensch, X-ray diffraction study of K₃NdSi₂O₇: a new framework silicate with a linear Si—O—Si bond, *Acta Crystallogr. B* 56 (2000) 773–779, <https://doi.org/10.1107/S0108768100006704>.
- [7] M. Wierzbicka-Wieczorek, U. Kolitsch, E. Tillmanns, The crystal structures of three new complex silicates of scandium, *Can. Mineral.* 48 (2010) 51–68, <https://doi.org/10.3749/canmin.48.1.51>.
- [8] M. Wierzbicka-Wieczorek, P.K. Krug, U. Kolitsch, High-temperature flux growth as a tool for the preparation of mixed-framework metal-Y silicates: a systematic evaluation of the influence of experimental parameters, *Cryst. Growth Des.* 17 (2017) 590–603, <https://doi.org/10.1021/acs.cgd.6b01448>.
- [9] S.M. Haile, B.J. Wuensch, T. Siegrist, R.A. Laudise, Conductivity and crystallography of new alkali rare-earth silicates synthesized as possible fast-ion conductors, *Solid State Ionics* 53 (1992) 1292–1301, [https://doi.org/10.1016/0167-2738\(92\)90328-M](https://doi.org/10.1016/0167-2738(92)90328-M).
- [10] C. Cascales, C. Zaldo, Crystal-field analysis of Eu³⁺ energy levels in the new rare-earth R BiY_{1-x}R_xGeO₅ oxide, *J. Solid State Chem.* 171 (2003) 262–267, [https://doi.org/10.1016/S0022-4596\(02\)00173-1](https://doi.org/10.1016/S0022-4596(02)00173-1).
- [11] M. Goyot, B. Ille, P. Lebrun, J.P. Martin, Performances of a preamplifier-silicon photodiode readout system associated with large BGO crystal scintillators, *Nucl. Instrum. Methods Phys. Res. Sect. Accel. Spectrom. Detect. Assoc. Equip.* 263 (1988) 180–187, [https://doi.org/10.1016/0168-9002\(88\)91032-7](https://doi.org/10.1016/0168-9002(88)91032-7).
- [12] X. Zhao, T. Yan, K. Wang, Y. Yan, B. Zou, J. Yu, R. Xu, NaEu₃(GeO₄)₂(OH)₂: a high-pressure-stable photoluminescent lanthanide germanate, *Eur. J. Inorg. Chem.* 2012 (2012) 2527–2532, <https://doi.org/10.1002/ejic.201200200>.
- [13] M. Emirdag-Eanes, M. Krawiec, J.W. Kolis, Hydrothermal synthesis and structural characterization of NaLnGeO₄ (Ln = Ho, Er, Tb, Tm, Yb, Lu) family of lanthanide germanates, *J. Chem. Crystallogr.* 31 (2001) 281–285, <https://doi.org/10.1023/A:1014378729117>.
- [14] J. Yeon, J.B. Hardaway, A.S. Sefat, A.M. Latshaw, H.-C. zur Loye, Crystal growth, structures, magnetic and photoluminescent properties of NaLnGeO₄ (Ln = Sm, Eu, Gd, Tb), *Solid State Sci.* 34 (2014) 24–30, <https://doi.org/10.1016/j.solidstatedsci.2014.05.002>.
- [15] O.A. Lipina, L.L. Surat, A.P. Tyutyunnik, A.N. Enyashin, A.Y. Chufarov, V.G. Zubkov, Structure and optical properties of KLa₉(GeO₄)₆O₂ and KLa_{8.37}Eu_{0.63}(GeO₄)₆O₂, *Chem. Phys. Lett.* 667 (2017) 9–14, <https://doi.org/10.1016/j.cplett.2016.11.021>.
- [16] A.M. Latshaw, B.O. Wilkins, G. Morrison, M.D. Smith, H.-C. zur Loye, A₅RE₄X[TO₄]₄ crystal growth: fluoride flux synthesis of Na₅Ln₄F[GeO₄]₄ (Ln=Pr, Nd), the first quaternary germanate oxyfluorides, *J. Solid State Chem.* 239 (2016) 200–203, <https://doi.org/10.1016/j.jssc.2016.04.038>.
- [17] K. Hughey, J. Yeon, H.-C. zur Loye, Crystal growth and structure determination of the new neodymium germanate, Na₂NdGeO₄(OH), *J. Chem. Crystallogr.* 44 (2014) 320–323, <https://doi.org/10.1007/s10870-014-0517-3>.
- [18] K. Hughey, J. Yeon, H.-C. zur Loye, Crystal growth and structure determination of the new neodymium germanate, Na₅Nd₄Ge₄O₁₆(OH), *J. Chem. Crystallogr.* 44 (2014) 376–379, <https://doi.org/10.1007/s10870-014-0525-3>.
- [19] K. Fulle, L.D. Sanjeewa, C.D. McMillen, Y. Wen, A.C. Rajamanthrilage, J.N. Anker, G. Chumanov, J.W. Kolis, One-pot hydrothermal synthesis of Tb^{III}₁₃(GeO₄)₆O₇(OH) and K₂Tb^{IV}Ge₂O₇: preparation of a stable terbium(4+) complex, *Inorg. Chem.* 56 (2017) 6044–6047, <https://doi.org/10.1021/acs.inorgchem.7b00821>.
- [20] P.-L. Chen, P.-Y. Chiang, H.-C. Yeh, B.-C. Chang, K.-H. Lii, Synthesis, crystal structure, magnetic and luminescence properties of KEuGe₂O₆: a europium cyclogermanate containing infinite chains of edge-sharing Eu–O polyhedra, *Dalton Trans.* 0 (2008) 1721–1726, <https://doi.org/10.1039/B716654K>.
- [21] U.W. Becker, J. Felsche, Phases and structural relations of the rare earth germanates RE₂Ge₂O₇, RE = La–Lu, *J. Common Met.* 128 (1987) 269–280, [https://doi.org/10.1016/0022-5088\(87\)90215-3](https://doi.org/10.1016/0022-5088(87)90215-3).
- [22] F. Piccinelli, M. Pedroni, S. Cagliero, A. Speghini, M. Bettinelli, Structural study of Ca₂Gd₂Ge₂O₉ and optical spectroscopy of the Eu³⁺ dopant ion, *J. Solid State Chem.* 212 (2014) 180–184, <https://doi.org/10.1016/j.jssc.2014.01.025>.
- [23] F. Piccinelli, A. Lausi, M. Bettinelli, Structural investigation of the new Ca₃Ln₂Ge₃O₁₂ (Ln=Pr, Nd, Sm, Gd and Dy) compounds and luminescence spectroscopy of Ca₃Gd₂Ge₃O₁₂ doped with the Eu³⁺ ion, *J. Solid State Chem.* 205 (2013) 190–196, <https://doi.org/10.1016/j.jssc.2013.07.021>.
- [24] O.A. Lipina, L.L. Surat, M.A. Melkozerova, A.P. Tyutyunnik, I.I. Leonidov, V.G. Zubkov, Synthesis, crystal structure and luminescence properties of CaY_{2-x}Eu_xGe₃O₁₀ (x=0–2), *J. Solid State Chem.* 206 (2013) 117–121, <https://doi.org/10.1016/j.jssc.2013.08.002>.
- [25] V.G. Zubkov, N.V. Tarakina, I.I. Leonidov, A.P. Tyutyunnik, L.L. Surat, M.A. Melkozerova, E.V. Zabolotskaya, D.G. Kellerman, Synthesis and crystal structure of Ln₂M²⁺Ge₄O₁₂, Ln=rare-earth element or Y; M=Ca, Mn, Zn, *J. Solid State Chem.* 183 (2010) 1186–1193, <https://doi.org/10.1016/j.jssc.2010.03.027>.
- [26] M. Swaffer, P.R. Slater, R.K. Gover, T. Matsumura, R. Kanno, T. Kamiyama, La₂MgGeO₆: a novel Ge based perovskite synthesized under ambient pressure, *ChemInform* 33 (2002), 17–17.
- [27] Y. Ochi, H. Morikawa, F. Marumo, H. Nozaki, Structures and magnetic properties of rare earth compounds in the melilite group, *Yogyo-Kyokai-Shi* 91 (1983) 229–235.
- [28] P. Berastegui, S. Hull, F.J. Garcá Garcá, J. Grins, A structural investigation of La₂(GeO₄)O and alkaline-earth-doped La_{0.33}(GeO₄)₆O₂, *J. Solid State Chem.* 168 (2002) 294–305, <https://doi.org/10.1006/jssc.2002.9724>.
- [29] A.M. Latshaw, K.D. Hughey, M.D. Smith, J. Yeon, H.-C. zur Loye, Photoluminescent and magnetic properties of lanthanide containing apatites: Na_xLn_{10-x}(SiO₄)₆O_{2-y}F_y, Ca_xLn_{10-x}(SiO₄)₆O_{2-y}F_y (Ln = Eu, Gd, and Sm), Gd_{9.34}(SiO₄)₆O₂, and K_{1.32}Pr_{8.68}(SiO₄)₆O_{1.36}F_{0.64}, *Inorg. Chem.* 54 (2015) 876–884, <https://doi.org/10.1021/acs.20150185b>.
- [30] L.A. Bueno, A.S. Gouveia-Neto, E.B. da Costa, Y. Messaddeq, S.J.L. Ribeiro, Structural and spectroscopic study of oxyfluoride glasses and glass-ceramics using europium ion as a structural probe, *J. Phys. Condens. Matter* 20 (2008), 145201, <https://doi.org/10.1088/0953-8984/20/14/145201>.
- [31] A.S. Gouveia-Neto, E.B. da Costa, L.A. Bueno, S.J.L. Ribeiro, Intense red upconversion emission in infrared excited holmium-doped PbGeO₃-PbF₂-CdF₂ transparent glass ceramic, *J. Lumin.* 110 (2004) 79–84, <https://doi.org/10.1016/j.jlumin.2004.04.005>.
- [32] T. Ragin, M. Kochanowicz, J. Žmójda, D. Dorosz, Spectroscopic Properties of Bismuth-germanate Glasses Co-Doped with Erbium and Holmium Ions, 2014, <https://doi.org/10.1117/12.2067063>, 92280C–92280C–8.
- [33] C.D. McMillen, J.W. Kolis, Hydrothermal synthesis as a route to mineralogically-inspired structures, *Dalton Trans.* 45 (2016) 2772–2784, <https://doi.org/10.1039/C5DT03424H>.
- [34] Apex3, Bruker AXS Inc., Madison, WI, 2015 (n.d.).
- [35] G.M. Sheldrick, Crystal structure refinement with SHELXL, *Acta Crystallogr. Sect. C Struct. Chem.* 71 (2015) 3–8, <https://doi.org/10.1107/S2053229614024218>.
- [36] G.M. Sheldrick, Cell Now, Georg-August-Universität Göttingen, Göttingen, Germany, 2008.
- [37] N.E. Brese, M. O'Keeffe, Bond-valence parameters for solids, *Acta Crystallogr. B* 47 (1991) 192–197, <https://doi.org/10.1107/S0108768190011041>.
- [38] I.D. Brown, D. Altermatt, Bond-valence parameters obtained from a systematic analysis of the inorganic crystal structure database, *Acta Crystallogr. B* 41 (1985) 244–247, <https://doi.org/10.1107/S0108768185002063>.
- [39] A. Orera, M.L. Sanjuán, E. Kendrick, V.M. Orera, P.R. Slater, Raman spectroscopy studies of apatite-type germanate oxide ion conductors: correlation with interstitial oxide ion location and conduction, *J. Mater. Chem.* 20 (2010) 2170–2175, <https://doi.org/10.1039/B922834A>.
- [40] E. Kroumova, M.I. Aroyo, J.M. Perez-Mato, A. Kirov, C. Capillas, S. Ivantchev, H. Wondratschek, Bilbao crystallographic server: useful databases and tools for phase-transition studies, *Phase Transit.* 76 (2003) 155–170, <https://doi.org/10.1080/0141159031000076110>.
- [41] M. Wierzbicka-Wieczorek, U. Kolitsch, G. Panczer, G. Giester, C. Chanmuang,

- A. Grzechnik, Crystal structures and photoluminescence properties of two novel sorosilicates with an unprecedented ratio of di- and trisilicate groups: $\text{Ba}_2\text{Ho}_{10}(\text{Si}_2\text{O}_7)_3(\text{Si}_3\text{O}_{10})_2$ and isotypic $\text{Ba}_2\text{Er}_{10}(\text{Si}_2\text{O}_7)_3(\text{Si}_3\text{O}_{10})_2$, *J. Solid State Chem.* 252 (2017) 33–42, <https://doi.org/10.1016/j.jssc.2017.05.004>.
- [42] K. Fulle, L.D. Sanjeewa, C.D. McMillen, J.W. Kolis, K. Fulle, L.D. Sanjeewa, C.D. McMillen, J.W. Kolis, Crystal chemistry of the discrete tetrasilicate units with rare earth dimers: $\text{Ba}_2\text{RE}_2\text{Si}_4\text{O}_{12}\text{F}_2$ (RE = Er–Lu) and $\text{Ba}_2\text{RE}_2\text{Si}_4\text{O}_{13}$ (RE = Pr–Sm), *Acta Crystallogr. B* 2017 (2017) in press.
- [43] X. Ren, Q. Pan, J. Liu, Y. Li, F. Wang, J. Li, Y. Xu, L. Li, A family of germanates constructed from Ge7 clusters co-templated by metal complexes and organic/inorganic species, *CrystEngComm* 16 (2014) 9545–9554, <https://doi.org/10.1039/C4CE00671B>.
- [44] Q.B. Nguyen, K.-H. Lii, $\text{Cs}_4\text{UGe}_8\text{O}_{20}$: a tetravalent uranium germanate containing four- and five-coordinate germanium, *Inorg. Chem.* 50 (2011) 9936–9938, <https://doi.org/10.1021/ic201789f>.
- [45] Q.B. Nguyen, C.-L. Chen, Y.-W. Chiang, K.-H. Lii, $\text{Cs}_3\text{UGe}_7\text{O}_{18}$: a pentavalent uranium germanate containing four- and six-coordinate germanium, *Inorg. Chem.* 51 (2012) 3879–3882, <https://doi.org/10.1021/ic3000872>.
- [46] G. Adachi, N. Imanaka, The binary rare earth oxides, *Chem. Rev.* 98 (1998) 1479–1514, <https://doi.org/10.1021/cr940055h>.